



**HAL**  
open science

## Combustion properties of H<sub>2</sub>/N<sub>2</sub>/O<sub>2</sub>/steam mixtures

R. Grosseuvres, A. Comandini, A. Bentaib, Nabiha Chaumeix

► **To cite this version:**

R. Grosseuvres, A. Comandini, A. Bentaib, Nabiha Chaumeix. Combustion properties of H<sub>2</sub>/N<sub>2</sub>/O<sub>2</sub>/steam mixtures. Proceedings of the Combustion Institute, 2019, 37 (2), pp.1537-1546. 10.1016/j.proci.2018.06.082 . hal-02354674

**HAL Id: hal-02354674**

**<https://hal.science/hal-02354674v1>**

Submitted on 21 Oct 2021

**HAL** is a multi-disciplinary open access archive for the deposit and dissemination of scientific research documents, whether they are published or not. The documents may come from teaching and research institutions in France or abroad, or from public or private research centers.

L'archive ouverte pluridisciplinaire **HAL**, est destinée au dépôt et à la diffusion de documents scientifiques de niveau recherche, publiés ou non, émanant des établissements d'enseignement et de recherche français ou étrangers, des laboratoires publics ou privés.



Distributed under a Creative Commons Attribution - NonCommercial 4.0 International License

## Combustion properties of H<sub>2</sub>/N<sub>2</sub>/O<sub>2</sub>/Steam mixtures

R. Grosseuvres<sup>\*1</sup>, A. Comandini<sup>1</sup>, A. Bentaib<sup>2</sup>, N. Chaumeix<sup>1</sup>

<sup>1</sup>INSIS, CNRS, 1C avenue de la recherche scientifique, 45071 Orléans Cedex 2, France

<sup>2</sup>IRSN, 3 avenue de la division Leclerc, 92260 Fontenay-aux-roses, France

\*Corresponding Author:

Romain Grosseuvres PhD Student

INSIS, CNRS, 1C avenue de la recherche scientifique, 45071 Orléans Cedex 2, France

Phone : +(33) 2 38 25 54 60

Fax : +(33) 2 38 69 60 04

e-mail : [romain.grosseuvres@cnrs-orleans.fr](mailto:romain.grosseuvres@cnrs-orleans.fr)

Colloquium: Laminar Flames; Detonations, Explosions, and Supersonic Combustion

Word equivalent length of

main text:	3562 words
equations:	Eq(1) : 8 words
references:	822 words
figures + captions:	Fig. 1: 300 words
	Fig. 2: 236 words
	Fig. 3: 170 words
	Fig. 4: 256 words
	Fig. 5: 245 words
	Fig. 6: 211 words
	Fig. 7: 172 words
	Fig. 8: 174 words

Total Length of Paper: 6156 words (Method 1)

Supplemental material available

## Combustion properties of H<sub>2</sub>/N<sub>2</sub>/O<sub>2</sub>/Steam mixtures

R. Grosseuvres<sup>\*1</sup>, A. Comandini<sup>1</sup>, A. Bentaib<sup>2</sup>, N. Chaumeix<sup>1</sup>

<sup>1</sup>INSIS, CNRS, 1C avenue de la recherche scientifique, 45071 Orléans Cedex 2, France

<sup>2</sup>IRSN, 3 avenue de la division Leclerc, 92260 Fontenay-aux-roses, France

### Abstract

The present work reports new experimental and numerical results of the combustion properties of hydrogen based mixtures diluted by nitrogen and steam. Spherical expanding flames have been studied in a spherical bomb over a large domain of equivalence ratios, initial temperatures and dilutions at an initial pressure of 100 kPa ( $T_{ini}$ = 296, 363, 413 K; N<sub>2</sub>/O<sub>2</sub>=3.76, 5.67, 9; %Steam=0, 20, 30). From these experiments, the laminar flame speed  $S_L^\circ$ , the Markstein length  $L'$ , the activation energy  $E_a$  and the Zel'dovich  $\beta$  number have been determined. These parameters were also simulated using COSILAB<sup>®</sup> in order to verify the validity of the Mével et al. [1] detailed kinetic mechanism. Other parameters as the laminar flame thickness  $\delta$  and the effective Lewis number  $Le_{eff}$  were also simulated. These new results aim at providing an extended database that will be very useful in the hydrogen combustion hazard assessment for nuclear reactor power plant new design.

**Keywords:** nuclear safety; combustion parameters; laminar flame speed; hydrogen

## 1. Introduction

During severe accident in Pressurized Water Reactor (PWR), the interaction between the fuel rod and steam leads to the build-up of an explosive atmosphere inside the containment building [2]. This atmosphere is mainly composed of hydrogen, oxygen, nitrogen and water vapor. In case of an ignition by an energy source (electrical discharge spark, hot surface, etc.), a flame occurs and is capable to threaten the containment building. To assess such scenario, CFD codes permit to model flame propagation in equivalent environment [2-3]. Furthermore, under certain conditions the flame which is propagating in the containment building can accelerate and undergo transition to detonation [4-5]. For these reasons it is a need to determine the laminar flame speed of  $H_2/N_2/O_2$  mixtures. First because the laminar flame speed is one of the fundamental input data to the CFD codes. Then it permits to evaluate fundamental parameters (laminar flame thickness  $\delta$ , effective Lewis number  $Le_{eff}$ , overall activation energy  $E_a$ , Zel'dovich number  $\beta$ ) which are directly involved in the criterion of flame acceleration permitting to distinguish fast flames from slow flames [2,5]. Substantial work has been conducted to determine laminar flame speed of hydrogen/air mixtures in ambient conditions ( $T_{ini}=296-300K$ ;  $P_{ini}=100-101.3kPa$ ) [6-16]. Fewer experiments were performed at high temperature with or without steam. Some of them were directly addressed to the hydrogen/air mixtures [16-19] while some others concerned mixtures of syngas ( $H_2/CO$ ) on restricted equivalence ratio domain [20, 21] or stoichiometric hydrogen/oxygen mixture [22]. Then, also a limited number of studies have been conducted on the dilution with nitrogen [6, 9, 19, 23].

In the present investigation, new experimental data on the laminar flame speed were obtained using the spherical bomb method of  $H_2/N_2/O_2/Steam$  mixtures over a wide range of initial conditions ( $T_{ini}= 296, 363, 413 K$ ;  $P_{ini}= 100kPa$ ;  $N_2/O_2=3.76, 5.67, 9$ ; %mol.Steam=0, 20, 30). The fundamental parameters mentioned above were calculated from numerical simulations using the Mével mechanism [1] and some

of them were derived from the experimental data. For H<sub>2</sub>/Air mixtures at 296 K and H<sub>2</sub>/Air mixtures diluted with 20%mol.Steam at 363K several kinetic models (the model of Li [24] and the GRI-Mech 3.0 mechanism [25]) were used in order to compare their impact on these combustion parameters and on  $S_L^0$ .

## 2. Material and method

The experiments leading to the laminar flame speeds measurements were conducted in two different stainless steel spherical bombs. The first one [26] was used for ambient temperature studies (296K), and the second one [27] for high temperatures studies (363, 413K). These two vessels are similar, they differs only by their volume: 93L and 56L. Both vessels are made of two concentric spheres permitting the circulation of a heat transfer fluid in order to regulate the inside temperature. For the high temperatures studies, a septum injector nut is directly connected to the vessel for the liquid water injection. For both devices, two opposite quartz windows for optical observations are mounted. The spark- ignition of the mixture is realized by two thin tungsten electrodes located along a diameter of the sphere which are linked to a high voltage and adapted probes to monitor the input power. High frequency pressures transducers (Kistler 601A/6001) are mounted flush with the inner wall to measure the pressure during the combustion. To observe the flame propagation and measure the laminar burning velocity, a Z-type Schlieren arrangement and high-speed camera are employed.

Two different cameras were used: for  $S_L^0$  higher than 3m/s we used Phantom V2520 up to 39 000 image/s and for  $S_L^0$  lower than 3m/s we used Phantom V1610 up to 25 000 image/s. The flame radius is extracted from the images via a home-made code based on Matlab® [28] which detects the position of the flame front [27] with an uncertainty of  $\pm 1$ pixel. The spark triggers the camera recording, the measurement of the pressure and the input power via a TTL generator connected to the electrodes.

The mixtures were prepared directly in the bomb using the partial pressure method. All the gas components were supplied by Air Liquide (purity >99.9999%). The air is composed of 20.9% O<sub>2</sub> + 79.1% N<sub>2</sub>. For experiments with steam, water vapor was obtained by the vaporization of liquid water (distilled water). Each time, the water vapor partial pressure was checked to be less than the saturated value in order to make sure that all the liquid phase has evaporated. The partial pressures and the initial total pressure were measured using different capacitance manometers: MKS 690A Baratron and MKS 631. The uncertainties on the equivalence ratio and on the steam molar fraction are respectively  $\pm 0.8\%$  and  $\pm 0.15\%$ . For experiments conducted in the 93L bomb, considering the large vessel volume the 8 fans were used in order to mix the mixture during 2 minutes. After this time, fans were stopped and the mixture was resting during 5 minutes before the ignition in order to dissipate the turbulence induced by this mixing process. This time was considered to be sufficient since there was no significant difference in the measured laminar flame speed over 20 minutes of resting is reported in the Fig. S1 in the Supplemental material. In the same way for experiments conducted in the 56L bomb, mixtures were also resting during 5 minutes after the filling process to remove any turbulence [27]. The initial temperature was checked prior to the ignition. Experiments were conducted at initial pressure of 100 kPa and initial temperatures of 296, 363, 413 K.

The laminar flame speed is defined as the unburned gases velocity in a normal direction relative to the flame front. Considering an outwardly expanding flame, curvature and strain rate have to be considered to determine this velocity. Indeed, local stretch induces a modification of the flame front upstream flow [29]. From the flame front images obtained in the spherical bomb ((Fig. 1(a)) the flame radius is deduced from which one can easily calculate a burning speed  $V_S = dR_f/dt$ . Unstretched velocity  $V_S^0$  are determined considering a non-linear variation of the flame speed with the stretch rate. Several relations can be used [30-31]. In the present study, the non-linear equation proposed by Ronney and Sivashinsky

[32] and modified later by Kelley and Law [33] (noted NQ for Quasi-steady Nonlinear model in [31]) was used. The laminar flame speed  $S_L^\circ$  and the Markstein length are derived from the solution of the following equation [27, 34]:

$$\left(\frac{V_S}{V_S^0}\right)^2 \cdot \ln\left(\frac{V_S}{V_S^0}\right)^2 = -\frac{2L_b \cdot \kappa}{V_S^0} \quad (1)$$

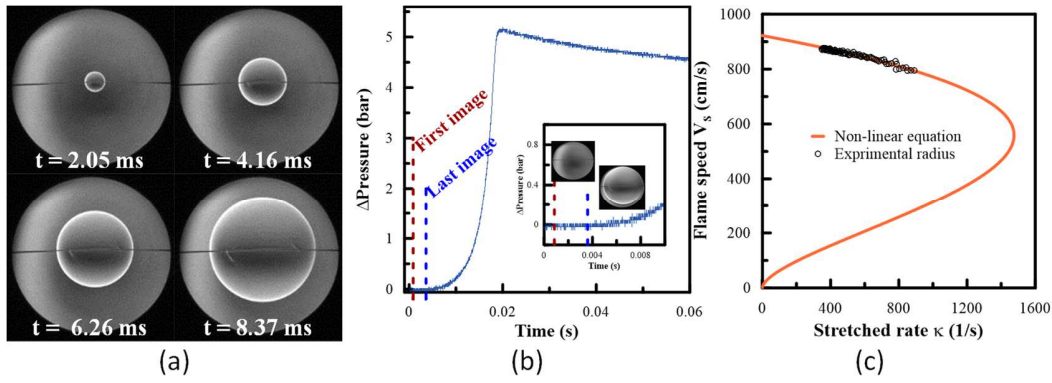


**Fig. 1.** Example of results for a  $H_2$ /air flame at  $\phi=3.6$ ,  $T_{ini}=296K$ ,  $P_{ini}=100kPa$ . (a): flame images, (b): recorded pressure profile, (c) flame speed versus stretch rate.

An example of the unstretched velocity extraction is given in Fig. 1(c). The range of experimental radius used in this data processing was from 10 to 70 mm in the 93L vessel and from 10 to 46 mm in the 56L vessel. The minimum radius was defined in order to remove the influence of the ignition energy while the maximum radius was chosen to avoid pressure effect on the laminar flame speed [35] (Fig. 1(b)). Since the pressure remains constant during the observation time, the laminar flame speed,  $S_L^\circ$  is determined by the ratio  $V_S^\circ/\sigma$ ,  $\sigma$  being the expansion ratio ( $=\rho_u/\rho_b$ ). The densities of the unburned and burned gases (respectively  $\rho_u$  and  $\rho_b$ ) are calculated by using the equilibrium code of COSILAB® [36].

### 3. Numerical calculations

To establish criterion of flame acceleration for the safety analysis, the combustion parameters ( $\delta$ ,  $Le_{eff}$ ,  $E_a$ ,  $\beta$ ) of  $H_2/N_2/O_2/Steam$  mixtures have to be determined by the laminar flame speeds simulations. Therefore, the detailed kinetic mechanism which should be used has to be selected based on his capability to reproduce experimental results for  $H_2/N_2/O_2$  mixtures over a wide range of initial conditions. For the present study, the Mével mechanism was used [1] because of its validation against a variety of experimental results for  $H_2/N_2/O_2$  mixtures [37] (laminar flame speeds, ignition delay times, detonation velocities and detonation cells widths). These simulations were conducted by using the one dimensional freely propagating flame code of COSILAB® [36].

Following the Zel'dovich analysis [38], The activation energy is the slope of the plot of  $2 \cdot \ln S_L^0 = f(1/T_b)$ .

To calculate the Lewis number of our mixtures, the definition corresponding of a weighted average of the reactants Lewis number was used [39].

## 4. Results and discussion

### 4.1. Laminar flame speed uncertainties

Many parameters can be potential uncertainties on the laminar flame speed determination from a spherical expanding flame [31, 40-41]. These parameters were carefully taken into account in the present study: experimental conditions, radiative heat losses and extrapolation process. This section presents how these uncertainties sources were fixed in order to assess the accuracy of the experimental results.

#### 4.1.1 Experimental conditions

For each experiment, the initial conditions were well-known ( $\Delta P_{ini} = \pm 0.5 \text{ kPa}$ ,  $\Delta T_{ini} = \pm 1 \text{ K}$ ,  $\Delta \phi = \pm 0.8\%$ ). The ignition energy for each test was measured (10mJ maximum). There had been very careful



consideration of the electrodes implementation (alignment, gap between the tips, diameters) in order to reduce flame-electrodes interactions.

#### 4.1.2 Radiative heat losses

Radiative heat losses can lead to a decrease of the flame speed [42]. In the present study, in order to verify that flames were not greatly influenced by radiation, the equation proposed in [43] was used to calculate the radiation-corrected flame speed. Results are presented in Fig. 2. One can see that differences between laminar flame speed experimentally obtained and radiation-corrected flame speed varies from 0.37 to 0.67 cm/s leading to a maximum uncertainty of 2%. Furthermore it was also checked that any bending was observed on flame speed profiles (Fig. 1(c)). Indeed as investigated in [44], bending on the flame speed profiles is a characteristic of flames which are greatly affected by the radiation effects.

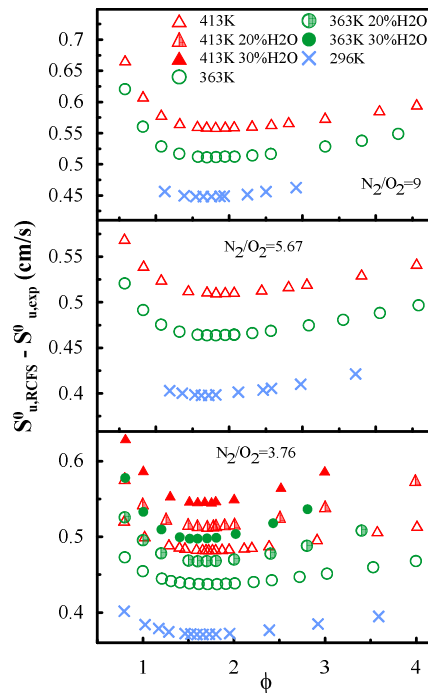


**Fig. 2.** Evaluation of the radiation-corrected flame speed according to [43].

### 4.1.3 Extrapolation process

As aforementioned in the previous section, different relations can be used to extract the unstretched velocity  $V_s^0$  using the spherical expanding flame method [30-31]. To verify that the present data are not impacted by the extrapolation method, the four extrapolation methods have been used to derive  $V_s^0$  obtained at 413K for H<sub>2</sub>/Air mixture: Linear model based on curvature (LC), Linear model based on stretch (LS), Nonlinear model with 3 fitting parameters (N3P), Nonlinear model in expansion form (NE) and Quasi-steady nonlinear model (NQ) (notations based on the one used in [31]). The results obtained with these different models are presented in Fig. 3. It is visible that all the models give very close results on the entire equivalence ratio domain, with a maximum standard deviation (9.65cm/s) obtained at  $\phi=2.11$ . We can also notice that the uncertainties of the results obtained with the model used in the present study (NQ) encompass the results obtained from the other results. This good agreement is due to the large radii used here to derive the laminar flame speed [30]. The impact of the extrapolation process can also be studied by using the relation proposed in [31] which corresponds to the product between the Markstein number (obtained using the LS model) and the Karlovitz number calculated at the middle radius for each experiment. Wu et al. [31] showed that to minimize extrapolation uncertainties, experiments should be conducted in the range of  $-0.05 < Ma_{\text{linear}} \cdot Ka_{\text{middle}} < 0.15$ . The product  $Ma_{\text{linear}} \cdot Ka_{\text{middle}}$  was calculated for all experiments conducted in the present study and reported with these limits in Fig. 3. One can see that only few experiments in lean and rich conditions may be slightly less accurate due to non-unity values of the Lewis number [31].

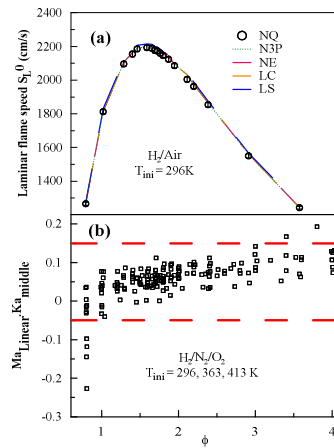


**Fig. 3.** Extrapolation models on  $S_L^0$  (a) and  $\{Ma_{linear} \times Ka_{middle}\}$  parameter (b) for  $H_2/Air$  mixtures,  $T_{ini}=296K, 363K, 413K$ ,  $P_{ini}=100kPa$ .

#### 4.2. Laminar flame speed and Markstein lengths

The laminar flame speeds obtained from the spherical bomb method are reported in Fig. 4 for the three initial temperatures and the three ratios  $N_2/O_2$  investigated. Results obtained for  $H_2/Air$  mixtures at 363K and 413K with 20 and 30%mol. of steam are also reported. It has to be noted that for  $N_2/O_2=9$  at  $T_{ini}=296K$  and for  $N_2/O_2=3.76$  at  $T_{ini}=363$  and 413K, investigated domain of  $\phi$  was reduced due to non-ignitable mixtures in rich conditions. Results obtained for  $H_2/Air$  mixtures at 296K were compared with the literature ones. This comparison is reported in the Supplemental material, Fig. S2. In each case, the maximum of the laminar flame speed is obtained for equivalence ratio between 1.6 and 1.8. As expected, the flame speed increases with increasing the initial temperature and decreasing ratio  $N_2/O_2$  (nitrogen playing the role of diluent). For a fix ratio  $N_2/O_2=3.76$  the steam dilution presents also a strong impact on the speed profile. In average  $S_L^0$  decreases of 41-42% or 62-65% when 20%mol. or 30%mol. of steam is added to the  $H_2/Air$  mixtures at 363K and 413K. Fig. 4 also contains the simulated  $S_L^0$  obtained with Mével mechanism [1]. Overall the simulation results follow the same trend as the experimental results. They are in very good agreement for lean and stoichiometric mixtures in dry

conditions, and for ultra-rich mixtures with steam. Nevertheless, two other kinetic mechanisms [24-25] were used in order to operate a comparison on the laminar flame speed for H<sub>2</sub>/Air mixtures at 296K and H<sub>2</sub>/Air mixtures diluted with 20%mol.Steam at 363K. The comparison between the results from these numerical calculations is reported in the Supplemental material, Fig. S3. For dry and wet cases, the models results are quite in agreement with  $S_L^0$  obtained experimentally. For H<sub>2</sub>/Air mixtures at 296K large discrepancies can be observed for lean mixtures between experimental and numerical results. Indeed for all the reaction models these differences oscillate between 8.9 and 11.8%. Better agreements are obtained for the largest laminar flame speeds ( $1.4 \leq \phi \leq 1.8$ ) while divergences increase for ultra-rich mixtures except with the GRI kinetic mechanism at  $\phi=2.4$  and  $\phi=2.9$  where the differences are lower than 4.5cm/s. Considering the experimental errors, the Li model presents the best predictions with an average error around 3%. For H<sub>2</sub>/Air/Steam mixtures at 363K, all the reaction models underestimate the laminar flame speeds although they present the same trend as the experimental results. This can be explained by the fact that radiations effect is not taking into account in the simulations. Indeed, radiations absorption by fresh gases plays an important role in enhancing  $S_L^0$  especially with three atomic molecules like water vapor which heat capacity is important. However, it appears that the Mével reaction model permits to present the best predictions on the entire equivalence ratio domain with an average error of 7.1%.

Eq(1) permits also to obtain the burned gases Markstein length  $L_B$  and consequently the unburned gases Markstein length  $L'$  ( $L'=L_B/\sigma$ ). For the experimental sets in Fig. 4,  $L'$  are reported in Fig. 5. Except for certain flames in lean mixtures (especially for mixtures diluted with steam), one can see that for each initial condition on almost the entire range of equivalence ratio studied flames are stable ( $L'>0$ ). While the initial temperature does not affect the response of the flame to the stretch, it appears that increasing the nitrogen dilution (increasing ratio N<sub>2</sub>/O<sub>2</sub>) leads to an increase of the instabilities for lean and

stoichiometric mixtures. As an example, for stoichiometric mixtures  $L'$  is becoming negative when  $N_2/O_2$  is increasing from 3.76 to 9. For  $N_2/O_2=3.76$ , the steam dilution appears to have a stronger impact on the Markstein length, making unstable flame from lean mixtures and more stable flame from ultra-rich ( $\phi > 2$ ) mixtures.

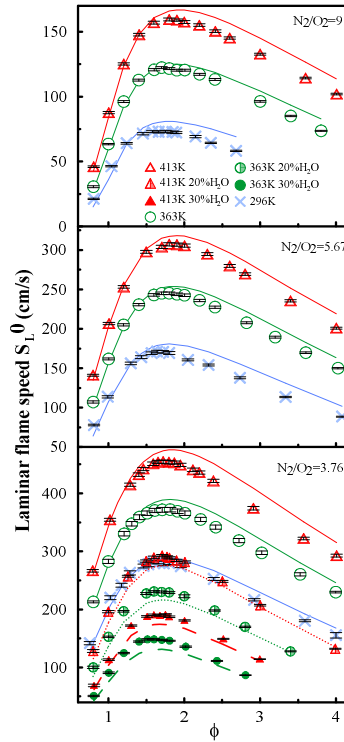


**Fig. 4.** Laminar flame speeds of  $H_2/N_2/O_2/Steam$  mixtures,  $T_{ini}=296K, 363K, 413K, P_{ini}=100kPa$ . Symbols: experiments; Lines: simulations.

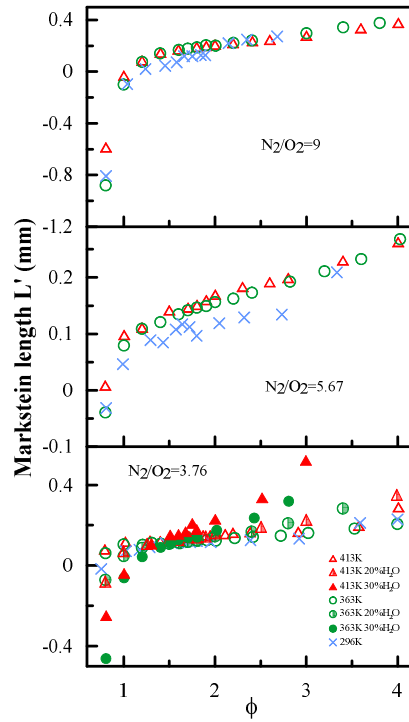


**Fig. 5.** Markstein lengths  $L'$  of  $H_2/N_2/O_2/$ Steam mixtures,  $T_{ini}=296K, 363K, 413K, P_{ini}=100kPa$ .

As mentioned previously, combustion parameters for safety analyses are inferred from laminar flame speeds such as the laminar flame, the thickness  $\delta$ , the effective Lewis number  $Le_{eff}$ , the overall activation energy  $E_a$  and consequently the Zel'dovich number  $\beta$ .

### 4.3. Laminar flame thickness

The definition of the flame thickness can be based on the thermal diffusivity ( $\delta_{therm}=\lambda\rho.C_p.S_L^0$ ) or on gradient of temperature ( $\delta_{gradT}=(T_{burned\ gases}-T_{unburned\ gases})/(dT/dx)_{max}$ ). 1-D simulation was operated in order to obtain the flame temperature profile and the other thermal parameters. Fig. 6 reports the values of  $\delta_{gradT}$  for the mixtures considered in the present study while  $\delta_{therm}$  is reported in the Supplemental material, Fig. S4.

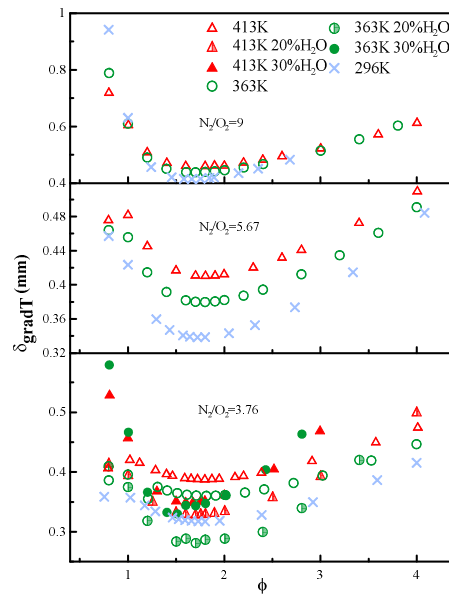


**Fig. 6.** Calculated  $\delta_{\text{gradT}}$  of  $\text{H}_2/\text{N}_2/\text{O}_2/\text{Steam}$  mixtures with the Mével model,  $T_{\text{ini}}=296\text{K}$ ,  $363\text{K}$ ,  $413\text{K}$ ,  $P_{\text{ini}}=100\text{kPa}$ .

The results from the two methods can present important differences. Indeed, the calculation using the temperature gradient leads to thicknesses higher than the ones calculated from the thermal diffusivity by a factor between 4.17 to 19.64. It can be noted for both flame thickness calculations the ratio  $\text{N}_2/\text{O}_2$  is the parameter which has the most influence. For the calculation based on thermal diffusivity, the temperature appears to have a minor impact except for the ratio  $\text{N}_2/\text{O}_2=9$  where the lowest temperature leads to have the thicker flame. On contrary, for the calculation based on gradient of temperature a measurable variation is observed when the initial temperature is varied and the maximum flame thickness is obtained at 413K.

As for  $S_L^0$ , laminar flame thicknesses were also calculated with two others kinetic mechanisms for  $\text{H}_2/\text{Air}$  mixtures at 296K and  $\text{H}_2/\text{Air}$  mixtures diluted with 20%mol.Steam at 363K in order to study the impact of the kinetic model. A comparison between the numerical results is presented in the Supplemental material, Fig. S5. One can see as in the previous results that for each reaction model,  $\delta_{\text{gradT}}$  always gives much larger values than  $\delta_{\text{therm}}$ . For dry and wet mixtures all the mechanisms present very

similar  $\delta_{\text{therm}}$  excepted for lean and ultra-rich mixtures while noticeable differences can be noted on  $\delta_{\text{gradT}}$ . For H<sub>2</sub>/Air mixtures at 296K, the models of Mével and Li provide comparable results whereas the GRI mechanism gives always lower values excepted at  $\phi=3.5$  and 4. For H<sub>2</sub>/Air/Steam mixtures at 363K,  $\delta_{\text{gradT}}$  can present large variations (from 29.5 to 90.4 $\mu\text{m}$ ) according to the kinetic mechanism used.

#### 4.4. Effective Lewis number

Fig. 7 reports the values of Effective Lewis numbers for the mixtures considered in the present study. The Lewis numbers of the reactants (H<sub>2</sub> and O<sub>2</sub>) are also figuring in order to illustrate that the  $Le_{\text{eff}}$  of the mixture is driven by  $Le_{\text{H}_2}$  in lean conditions and by  $Le_{\text{O}_2}$  in rich conditions [39].

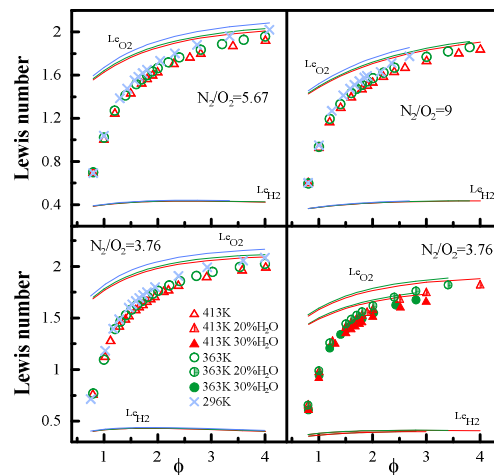


**Fig. 7.** Effective Lewis numbers of H<sub>2</sub>/N<sub>2</sub>/O<sub>2</sub>/Steam mixtures,  $T_{\text{ini}}=296\text{K}, 363\text{K}, 413\text{K}$ ,  $P_{\text{ini}}=100\text{kPa}$ .

Following the trend of  $L'$  (Fig.5), it has to be noted that the majority of the studied flames are stable ( $Le_{\text{eff}} > 1$ ) except for some conditions ( $\phi=1$  at  $N_2/O_2=3.76$  with 20%mol.Steam,  $\phi=1$  at  $N_2/O_2=9$  and also for lean mixtures in every conditions). It is also visible that the dilution by N<sub>2</sub> (increasing ratio  $N_2/O_2$ ) or



by steam leads to a decrease of the  $Le_{eff}$ . In particular we can notice stoichiometric mixtures which are becoming unstables ( $Le_{eff} < 1$ ) when the ratio  $N_2/O_2$  increases from 5.67 to 9 or when the steam is added.

#### 4.5. Overall activation energy and Zel'dovich number

Calculation results of the Overall Activation Energy are reported in the Supplemental material, Fig. S6. The evolution of  $\beta$  with the equivalence ratio is presented in Fig. 8. In each case, the minimum of  $\beta$  is obtained at the equivalence ratio for which the laminar flame speed is the highest one. As it could be intuitively predicted, the reactivity of the mixtures of interest increases with the temperature and decreases with the dilution by nitrogen or steam. The decrease of  $\beta$  with the initial temperature increases when the dilution by  $N_2$  increases. The average decreasing at  $N_2/O_2=3.76$  is around 13.1% while it is approximately 22.6% at  $N_2/O_2=9$ .

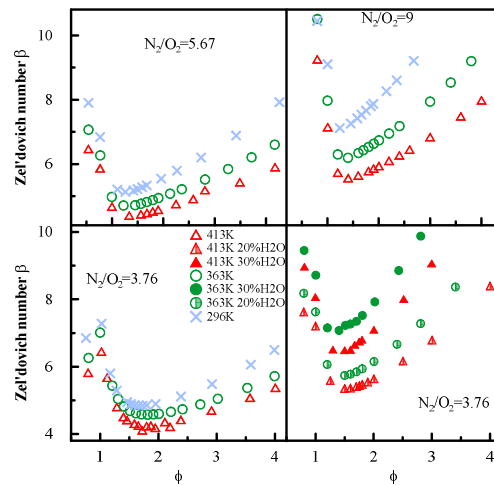


**Fig. 8.** Calculated Zel'dovich numbers of  $H_2/N_2/O_2/Steam$  mixtures,  $T_{ini}=296K, 363K, 413K, P_{ini}=100kPa$ .

The model dependency of  $\beta$  can be studied with the Figure S7 in the Supplemental material where numerical results from the mechanisms of Li, Mével and GRI 3.0 are presented for  $H_2/Air$  mixtures at 296K and  $H_2/Air$  mixtures diluted with 20%mol.Steam at 363K. As for the laminar flame thickness  $\delta_{therm}$ , the reaction models of Mével and Li present quite similar  $\beta$  for dry and wet mixtures. From the

GRI mechanism,  $\beta$  is always higher on the entire domain of equivalence ratio. Furthermore, the results from the Mével model are always the smallest ones except at  $\phi=2.9, 3.6$  and  $4$  for  $H_2/Air$  mixtures at  $296K$  and at  $\phi=0.8$  for  $H_2/Air/Steam$  mixtures at  $363K$ .

For dry mixtures  $\beta$  was also derived from  $S_L^0$  obtained experimentally. A comparison between the  $\beta$  derived from experiments and the one obtained numerically with Mével model is reported in the Supplemental material, Fig. S8. In order to increase the number of data, a fit was applied on the experimental curve  $S_L^0=f(\phi)$  as reported in the Supplemental material, Fig. S9. As one can see, trends are very well reproduced with the mechanism for ratios  $N_2/O_2=5.67$  and  $9$ . Furthermore, an excellent agreement can be observed at  $363$  and  $413K$  for  $N_2/O_2=5.67$  while for  $N_2/O_2=9$ ,  $\beta$  is always slightly overpredicted. For  $N_2/O_2=3.76$  and  $T_{ini}=296K$ , results from simulation are shifted toward the richer mixtures, whereas at  $363$  and  $413K$  large discrepancies and an excellent agreement can be noticed respectively for  $\phi < 2$  and  $\phi \geq 2$ .

## 5. Conclusions

Expanding spherical flames of  $H_2/N_2/O_2$  mixtures have been studied for a wide range of equivalence ratios  $\phi$  ( $0.8 \leq \phi \leq 4$ ), initial temperatures ( $296, 363$  and  $413K$ ) and  $N_2/O_2$  ratios ( $3.76, 5.67, 9$ ) at  $100$  kPa. From these experiments,  $S_L^0, L'$  have been determined. Moreover, the effect of steam addition to the mixtures was also investigated ( $20, 30\%$  mol of steam). Higher temperatures and ratio  $N_2/O_2$  promote faster flame propagation while steam addition has a suppressing effect. Mével chemical kinetic model was used in order to simulate laminar flame speeds in the same initial conditions and was compared to the results. Good agreements between experimental and simulated results were observed. This validation demonstrates that this model can be used to simulate premixed flame properties relevant to combustion hazard evaluation in NPP [45]. Moreover,  $S_L^0$  is also important for the use of CFD codes where it is used as a normalizing parameter for the determination of the turbulent flame speed. The model was

subsequently used to perform calculations of the following parameters: laminar flame, thickness  $\delta$ , effective Lewis number  $Le_{eff}$ , overall activation energy  $E_a$ , Zel'dovich number  $\beta$ . These new data permit to estimate the flame acceleration criterion in case of mixtures diluted with water vapor.

### **Acknowledgements**

The present study was funded by Programme Investissement d'Avenir- MITHYGENE Grant agreement n°ANR 11-RSNR-0015.

## References

- [1] R. Mével, S. Javoy, F. Lafosse, N. Chaumeix, G. Dupré, C.E. Paillard, *Proc. Combust. Inst.* 32 (2009) 359-366.
- [2] A. Bentaïb, N. Meynet, A. Bleyer, *Nucl. Eng. Technol.* 47 (2015) 26-32.
- [3] A. Bleyer, J. Taveau, N. Djebaili-Chaumeix, C. E. Paillard, A. Bentaïb, *Nucl. Eng. Des.* 245 (2012) 189-196.
- [4] A. Bentaib, A. Bleyer, N. Meynet, N. Chaumeix, B. Schramm, M. Höhne, P. Kostka, M. Movahed, S. Worapittayaporn, T. Brähler, H. Seok-Kang, M. Povilaitis, I. Kljenak, P. Sathiah, *Ann. Nucl. Energy* 74 (2014) 143-152.
- [5] S. Dorofeev, M. Kuznetsov, V. Alekseev, A. Efimenko, W. Breitung, *J. Loss Prev. Proc. Ind.* 14 (2001) 583-289.
- [6] D. Dowdy, D. Smith, S. Taylor, *Proc. Combust. Inst.* (1990) 325-332.
- [7] F. Egolfopoulos, C.K. Law, *Proc. Combust. Inst.* (1990) 333-340.
- [8] G. Koroll, R. Kumar, E. Bowles, *Combust. Flame* 94 (1993) 330-340.
- [9] K. Aung, M. Hassan, G. Faeth, *Combust. Flame* 109 (1997) 1-24.
- [10] S. Tse, D. Zhu, C.K. Law, *Proc. Combust. Inst.* 28 (2000) 1793-1800.
- [11] N. Lamoureux, N. Djebaili-Chaumeix, C.E. Paillard, *Exp. Therm. Fluid Sci.* 27 (2003) 385-393.
- [12] Z. Huang, Y. Zhang, K. Zeng, B. Liu, Q. Wang, D. Jiang, *Combust. Flame* 146 (2006) 302-311.
- [13] C. Tang, Z. Huang, C. Jin, J. He, W. J., X. Wang, H. Miao, *Int. J. Hydrogen Energy* 33 (2008) 4906-4914.
- [14] E. Hu, Z. Huang, J. He, H. Miao, *Int. J. Hydrogen Energy* 34 (2009) 8741-8755.
- [15] G. Dayma, F. Halter, P. Dagaut, *Combust. Flame* 161 (2014) 2235-2241.
- [16] Z.-U. Sun, G.-X. Li, *Energy* 116 (2016) 116-127.

- [17] D. Liu, R. MacFarlane, *Combust. Flame*, 49 (1983) 59-71.
- [18] G. Koroll, S. Mulpuru, *Proc. Combust. Inst.* 21 (1986) 1811-1819.
- [19] N. Lamoureux, N. Djebaili-Chaumeix, C.E. Paillard, *Journal de Physique IV* 12 (2002) 7-445.
- [20] A.K. Das, K. Kumar, C.J. Sung, *Combust. Flame* 158 (2011) 345-353.
- [21] J. Santner, F.L. Dryer, Y. Ju, *Proc. Combust. Inst.* 34 (2013) 719-726.
- [22] M. Kuznetsov, R. Redlinger, W. Breitung, J. Grune, A. Friedrich, N. Ichikawa, *Proc. Combust. Inst.* 33 (2011) 895-903.
- [23] L. Qiao, C.H. Kim, G.M. Faeth, *Combust. Flame* 143 (2005) 79-96.
- [24] J. Li, Z. Zhao, A. Kazakov, M. Chaos, F.L. Dryer, J.J. Scire, Jr., *Int. J. Chem. Kinet.*, 39 (2007) 109-136.
- [25] G.P. Smith, D.M. Golden, M. Frenklach, N.W. Moriarty, B. Eiteneer, M. Goldenberg, C.T. Bowman, R.K. Hanson, S. Song, W.C. Gardiner, V.V. Lissianski, Z. Qin: GRI-Mech 3.0 available at [http://www.me.berkeley.edu/gri\\_mech/](http://www.me.berkeley.edu/gri_mech/).
- [26] J. Goulier, N. Chaumeix, F. Halter, N. Meynet, A. Bentaïb, *Nucl. Eng. Des.* 312 (2017) 214-227.
- [27] D. Nativel, M. Pelucchi, A. Frassoldati, A. Comandini, A. Cuoci, E. Ranzi, *Combust. Flame* 166 (2016) 1-18.
- [28] MATLAB. The Mathworks Incorporated, Version 2016b. [www.mathworks.com](http://www.mathworks.com).
- [29] R. Mével, F. Lafosse, N. Chaumeix, G. Dupré, C.E. Paillard, *Int. J. Hydrogen Energy* 34 (2009) 9007-9018.
- [30] Z. Chen, *Combust. Flame* 158 (2011) 291-300.
- [31] F. Wu, W. Liang, Z. Chen, Y. Ju, C.K. Law, *Proc. Combust. Inst.* 35 (2015) 663-670.
- [32] P. Ronney, G. Sivashinsky, *J. Appl. Math.* 49 (4) (1989) 1029-1046.
- [33] A. Kelley, C.K. Law, *Combust. Flame*, 156 (2009) 1844-1851.

- [34] A. Comandini, G. Pengloan, S. Abid, N. Chaumeix, *Combust. Flame* 173 (2016) 425-440.
- [35] M. Burke, Z. Chen, Y. Ju, F. Dryer, *Combust. Flame* 156 (2009) 771-779.
- [36] COSILAB. The Combustion Simulation Laboratory, Rotexo GmbH & Co. KG, Haan, Germany, 2009 Version 3.3.2. <http://www.SoftPredict.com>
- [37] R. Mével, J. Sabard, J. Lei, N. Chaumeix, *Int. J. Hydrogen Energy* 41 (2016) 6905-6916.
- [38] Y. Zel'dovich, *The mathematical theory of combustion and explosions*, Consultants Bureau, New York, 1985.
- [39] R. Addabbo, J. Bechtold, M. Matalon, *Proc. Combust. Inst.* 29 (2002) 1527-1535.
- [40] Z. Chen, *Combust. Flame* 162 (2015) 2442-2453.
- [41] E. Varea, J. Beeckmann, H. Pitsch, S. Chen, B. Renou, *Proc. Combust. Inst.* 35 (2015) 711-719
- [42] J. Santner, F. Haas, Y. Ju, F. Dryer, *Combust. Flame* 161 (2014) 147-153.
- [43] H. Yu, W. Han, J. Santner, X. Gou, C. Sohn, Y. Ju, Z. Chen, *Combust. Flame* 161 (2014) 2815-2824.
- [44] J. Jayachandran, R. Zhao, F. Egolfopoulos, *Combust. Flame* 161 (2014) 2305-2316.
- [45] W. Breitung, C. Chan, S. Dorofeev, A. Eder, B. Gelfand, M. Heitsch, R. Klein, A. Malliakos, E. Shepherd, E. Stude, P. Thibault, *Flame Acceleration and Deflagration-to-Detonation Transition in Nuclear Safety*, Report No. NEA/CSNI/R(2000)7

## List of Figures

Fig. 1. Example of results for a H<sub>2</sub>/air flame at  $\phi=3.6$ ,  $T_{ini}=296K$ ,  $P_{ini}=100kPa$ . (a): flame images, (b): recorded pressure profile, (c) flame speed versus stretch rate.

Fig. 2. Evaluation of the radiation-corrected flame speed according to [43].

Fig. 3. Extrapolation models on  $S_L^0$  (a) and  $\{M_{linear} \times K_{middle}\}$  parameter (b) for H<sub>2</sub>/Air mixtures,  $T_{ini}=296K$ , 363K, 413K,  $P_{ini}=100kPa$ .

Fig. 4. Laminar flame speeds of H<sub>2</sub>/N<sub>2</sub>/O<sub>2</sub>/Steam mixtures,  $T_{ini}=296K$ , 363K, 413K,  $P_{ini}=100kPa$ . Symbols: experiments; Lines: simulations.

Fig. 5. Markstein lengths  $L'$  of H<sub>2</sub>/N<sub>2</sub>/O<sub>2</sub>/Steam mixtures,  $T_{ini}=296K$ , 363K, 413K,  $P_{ini}=100kPa$ .

Fig. 6. Calculated  $\delta_{gradT}$  of H<sub>2</sub>/N<sub>2</sub>/O<sub>2</sub>/Steam mixtures with the Mével model,  $T_{ini}=296K$ , 363K, 413K,  $P_{ini}=100kPa$ .

Fig. 7. Effective Lewis numbers of H<sub>2</sub>/N<sub>2</sub>/O<sub>2</sub>/Steam mixtures,  $T_{ini}=296K$ , 363K, 413K,  $P_{ini}=100kPa$ .

Fig. 8. Calculated Zel'dovich numbers of H<sub>2</sub>/N<sub>2</sub>/O<sub>2</sub>/Steam mixtures,  $T_{ini}=296K$ , 363K, 413K,  $P_{ini}=100kPa$ .

## List of supplemental material

- Supplemental\_Material\_Combustion properties of H2 N2 O2 Steam mixtures.pdf
  - Fig. S1. Effect of resting time before ignition on measured laminar flame speed of H<sub>2</sub>/Air flame.
  - Fig. S2. Comparison of the experimental laminar flame speed for H<sub>2</sub>/Air mixtures of the present study with the results from literature.
  - Fig. S3. Comparison of laminar flame speeds obtained experimentally and numerically from three different kinetic models at P<sub>ini</sub>=100kPa for (a) H<sub>2</sub>/Air mixtures at T<sub>ini</sub>=296K and (b) H<sub>2</sub>/Air mixtures diluted with 20%mol.Steam at 363K.
  - Fig. S4. Calculated  $\chi_{therm}$  of H<sub>2</sub>/N<sub>2</sub>/O<sub>2</sub>/Steam mixtures with the Mével model, T<sub>ini</sub>=296K, 363K, 413K, P<sub>ini</sub>=100kPa.
  - Fig. S5. Comparison of laminar flame thickness obtained from various kinetic models at P<sub>ini</sub>=100kPa for (a) H<sub>2</sub>/Air mixtures at T<sub>ini</sub>=296K and (b) H<sub>2</sub>/Air mixtures diluted with 20%mol.Steam at 363K.
  - Fig. S6. Calculated Overall Activation Energy of H<sub>2</sub>/N<sub>2</sub>/O<sub>2</sub>/Steam mixtures, T<sub>ini</sub>=296K, 363K, 413K, P<sub>ini</sub>=100kPa
  - Fig. S7. Comparison of Zel'dovich number obtained from various kinetic models at P<sub>ini</sub>=100kPa for (a) H<sub>2</sub>/Air mixtures at T<sub>ini</sub>=296K and (b) H<sub>2</sub>/Air mixtures diluted with 20%mol.Steam at 363K.
  - Fig. S8. Zel'dovich number versus equivalence ratio for H<sub>2</sub>/N<sub>2</sub>/O<sub>2</sub> mixtures, T<sub>ini</sub>=296K, 363K, 413K, P<sub>ini</sub>=100kPa derived experimentally (symbol) and numerically (lines).